Understanding the link between the extreme weather conditions in central Europe in spring 2018 and a preceding record-breaking sea ice reduction in the Bering sea.

Author: FERRAN LÓPEZ MARTÍ
Supervisors: JUAN C. ACOSTA[1], juan.acosta@bsc.es; MARKUS G. DONAT[1], markus.donat@bsc.es; PABLO ORTEGA[1], pablo.ortega@bsc.es; SIMON WILD[1], simon.wild@bsc.es; RAÜL MARCOS[1,2], rmarcos@meteo.ub.edu*
[1] *Earth Sciences Department, Barcelona Supercomputing Center (BSC), Barcelona, Spain.*
[2] *Facultat de Física, Universitat de Barcelona, Diagonal 645, 08028 Barcelona, Spain.*

Abstract: This study examines a series of extreme weather events, including large-scale droughts and heatwaves, over Northern and Central Europe between April and June of 2018, and explores their potential link with an unprecedent low sea-ice anomaly in the Bering Sea during January-April of the same year. Analysis of observational and reanalysis data shows that the development of a persistent blocking pattern over Scandinavia is likely behind the occurrence of the extreme weather episodes in Europe. To asses if this and the extreme weather conditions are associated with the record-breaking sea-ice reduction in the Bering Sea, we have performed a composite analysis based on six similar previous events in the Bering Sea. One month after the driving sea-ice signal in March-April, the composite of geopotential height at 500 hPa reproduces a significant blocking pattern Southeast of Scandinavia, which persists during the next three months in the same way of the blocking in 2018, although slightly shifted. Additional composites based on surface temperature and precipitation show that general tendency towards drier and hotter conditions over the region of the blocking, and therefore also displaced with respect to those in 2018. These differences, however, could be accounted by internal variability effects, as the position of the blocking center of action moves slightly around for each of the individual composited years. Finally, these results allow us to suggest that a linkage between Bering Sea ice and Europe weather is plausible. We cannot, however, definitively conclude that a casual link exists between them, for which additional attribution studies based on climate models would be needed.

I. INTRODUCTION

During the spring and early summer of 2018, Central and Northern Europe experienced extremely dry and hot conditions reaching unprecedented levels and had a big socioeconomic impact. Due to this persistent weather situation, both renewable and conventional energy sources were affected, with huge effects on the run-of-river hydropower generation, most significantly in Sweden and Germany. The low river levels impacted river transport causing coal supply problems to power plants, and affected river cooled nuclear power plants having to shut down temporarily to protect the river environment because the level was too low to keep introducing hot water (*Agora Energiewende and Sandbag* 2019). By contrast, solar energy generation increased during the same period, wherein some parts of northern and central Europe had up to 40% more sunshine hours than average that year (*Copernicus* 2019). Germany achieved a record of solar production in July, producing 15.1% of the total electric production in the country (*Burger* 2018). Due to the drought and enhanced by the high temperatures, the agriculture sector experienced a yield reduction of the main crops up to 50% (*Toreti et al.* 2019). In June, dry and hot conditions favoured unprecedented forest fires in Scandinavia, affecting mainly in Sweden where the government had to call international assistance (*NASA Earth Observatory* 2018). During the second half of July, northern and central Europe suffered an extreme heatwave, with some record-breaking, that was intensified by the persistent conditions in the preceding months caused by a continuous circulation anomaly (*Yiou et al.* 2019).

From April to July, the circulation was characterized by high pressure conditions moving over Scandinavia, western Europe and the North Atlantic. The persistent and intense atmospheric blocking was essential for developing the large-scale heatwave and drought enhanced by the soil-moisture feedbacks (*Toreti et al.* 2019). Some studies show evidence that extreme events like this are favoured by amplified planetary waves (Rossby waves); this pattern was also observed during the European heatwaves of 2003, 2006 and 2015 and other extreme events (*Kornhuber et al.* 2019, *Screen and Simmonds* 2014). Amplification of planetary waves has been proposed as a possible mechanism linking mid-latitude weather extremes with the faster warming of the Arctic than the rest of the world, known as Arctic Amplification (*Screen and Simmonds* 2013b). Even though there is still no observational evidence that larger amplitude planetary waves are enhanced by the Arctic Amplification (*Barnes* 2013, *Screen and Simmonds* 2013a). Large-scale changes in the mid-latitude circulation have also been directly associated with sea-ice loss (*Budikova* 2009, *Overland and Wang* 2010). Ocean ice-free conditions when sea-ice retreats allow for larger air-sea exchanges of heat and moisture increasing the near-surface temperature and affecting the lower-troposphere by increasing the geopotential thickness. As the whole Arctic is warming, the poleward

* Electronic address: flopezma83@alumnes.ub.edu

thickness gradient between 1000-500 hPa is diminishing and therefore the upper-level zonal winds too, resulting in a lower progression and higher amplitude of the large-scale Rossby waves, and a northern elongation of ridges in 500 hPa waves enhancing the probability of extreme weather due to more prolonged weather conditions (*Francis and Vavrus* 2012).

It is widely accepted that sea-ice conditions in the Arctic play a role for mid-latitudes weather, although it is still not clear which mechanisms connects the two regions. This teleconnection is more pronounced during autumn and winter than during spring when the sea-ice coverage has spread again, and the positive feedbacks from the sea-ice retreat are not longer active (*Francis and Vavrus* 2012). An example of these Arctic influences is described in *Acosta Navarro et al.* (2019), linking a record low December 2016 precipitation event in Europe to extremely low sea-ice conditions in Barents and Kara Seas in the month before.

In this study, we aim to understand the possible relation between the extreme and persistent weather over Europe in 2018 and the record breaking reduced sea-ice conditions observed in the Bering sea from January to April of the same year, the lowest winter-maximum areal sea-ice coverage on record from 1980 (*Thoman JR et al.* 2019). In the following section we describe the different data sets and the methodology used. Section III characterizes the event and discusses it in the context of previous similar episodes. Finally, in section IV, we outline the main conclusions and consider future prospects.

II. DATA AND METHODS

A. Data

This analysis is exclusively based on monthly gridded observation and reanalysed products, to be able to characterise better the large-scale features of the 2018 event. We give preference to widely used long datasets to maximise the period for the identification of similar events. The longest time interval covered by all products is 1958-2018, which will be our analysis period.

1. Sea-ice data

The sea-ice state in the Arctic is characterized with sea-ice concentration (SIC) data describing the fraction over an area covered by sea-ice (in %). Two different datasets, both regridded onto a 1°x1° regular grid, are used to characterize the 2018 and assess the sensitivity to the observational record considered. These are the satellite-derived SSM/I (Special Sensor Microwave/Imager) SIC from CERSAT/IFREMER (Note1) for 1958-2018, which covers a longer time period by combining passive microwave satellite data and historical sources. Both SIC sources are compared for the Bering region during March-April in Figure 1 and discussed in section III.

2. Atmospheric data

The characterization of the conditions over Europe is done using monthly mean near-surface mean temperature [K], and total precipitation [m·s^1] from the observational data set E-OBS version 19.0e (*Haylock et al.* 2008). This product is derived from a spatial interpolation of daily climate observations from land-only stations. The data used is in a high-resolution regular grid data of 0,1° for the European region (25N-71.5N; 25W-45E) and covers the period from 1958 to 2018.

The mid-troposphere circulation over the northern hemisphere is characterised and analyzed using the geopotential height at 500 hPa (z500, in gpm) from the JRA-55 reanalysis (*Kobayashi et al.* 2015). This dataset starts in 1958, when the global scale radiosonde observations began, and has a spatial resolution of 1,25°. The monthly mean data for this variable is computed from 6 hourly frequency data.

B. Methods

All the scripts developed for analyzing the data and generating the plots and graphics have been done using the free software environment R (*R Core Team* 2019) and the "s2dverification" package (*Manubens et al.* 2018).

1. Event characterization

To determine the extremeness of the weather conditions from December 2017 to July 2018 have been compared with the climatological state between 1958-2017. Each variable is analyzed in a different way, depending on its characteristics.

The near-surface temperature variability follows approximately a Gaussian distribution, so its anomaly can be expressed and interpreted in standard deviation units. The standardized anomaly from the climatology (1958-2017) is calculated for each grid point following the next equation:

$$tas' = \frac{tas - \overline{tas}}{\sigma} \tag{1}$$

Precipitation has a very irregular distribution, and instead of computing its standardized anomaly, we weigh the total amount of precipitation by the long-term monthly climatology (i.e. with respect to 1958-2017) as a percentage as it follows:

$$prlr' = \frac{prlr}{\overline{prlr}} \cdot 100 \tag{2}$$

Finally, SIC and geopotential height at 500 hPa are not computed as standardized anomalies because we do not only want to assess the extremeness of the anomaly but to quantify how much anomalous it was, even though also have a good approximation to a Gaussian distribution like temperature. Thus, the anomaly from the mean climatology is computed as a single difference between the monthly mean minus the climatology (1958-2017 for the geopotential height and HadISST SIC, and 1992-2017 for CERSAT SIC).

2. *Composite analysis*

The main hypothesis we seek to confirm is if the conditions in the Bering sea favoured the occurrence of a blocking pattern over Europe, leading to the large-scale drought and heatwave in 2018. For this purpose, this study makes use, as already mentioned, of observational and reanalysis data for the period between 1958 to 2017 in order to look for similar events with comparable conditions, thus potentially showing the same linkage within the two regions. By doing so, a composite with the events with the closest sea-ice conditions in the Bering Sea to 2018 is performed. A composite is just an average of climate fields in years that meet a specific condition, in this case a low state in the sea-ice in the Bering sea.

In order to select the years more comparable to the 2018 conditions, a sea-ice state index for the Bering Sea is used. This Bering Sea Ice index (BSI) is computed as the area weighted regional mean of the SIC standardized anomalies in the northern Bering Sea (57-67N; 170-200E). The index is calculated as the average in March and April for the period 1958-2018 (Figure 1).

Excluding 2018, and using HadISST which is the longest record, the years within the 10^{th} percentile are selected. This corresponds to the six years with the lowest SIC in the region before 2018.

Finally, composites are computed for other variables as the average during those six years. To asses the response to the low sea-ice, the composites are computed also in two month periods, delayed from 0 to 3 months with respect to March and April, when the lowest sea-ice anomalies happened. That is, 1-month delay corresponds to April and May, 2-month to May-June, and 3-month to June-July. The composite anomaly fields are: the geopotential height at 500 hPa, surface temperature and precipitation.

The statistical significance of the different composites is evaluated with a bootstrap method (*Efron and Tibshirani* 1986). This test consists of randomly sampling 6 years from the 1958-2017 period to create an "alternative" composite not constrained by the sea-ice state, repeating the process 1000 times to have a control distribution of "alternative" composites. We can then assess where the Bering Sea Ice constrained composite lays with respect to the control distribution, from which a significance level can be set. We use a significance level of $p \leq 0.05$, leaving 2.5% on both sides of the distribution.

III. RESULTS AND DISCUSSION

A. Characterization of the event

1. *Observed sea-ice state*

Between January and April 2018, the Bering Sea experienced the most greatest sea-ice reduction in the whole Arctic, setting a new record of low sea-ice for the area in the observations and past reconstructions since 1850 (*Thoman JR et al.* 2019). The right hand panel of figure 1 shows the BSI time-series for March-April (computed over the purple box in the left panel) for the two datasets. The 2018 low-record is between 2 and 3 standard deviations lower than the climatological mean. Despite the difference in the magnitude of the anomaly, both datasets show unprecedented values, and their timeseries show a high correlation with a Pearson coefficient of 0.94 increasing confidence in the exceptional nature of the event.

The left-hand panel of figure 1 provides a spatial description of the event. It shows how SIC anomalies for March and April in the west and north of the Bering Sea reached values as low as -80% implying that this region, usually covered completely by sea-ice, was virtually ice free. February shows almost the same anomaly magnitude and distribution than the two following months, and January was less intense but still reaching SIC reductions of up to 60% with the same spatial distribution. Finally, May is the month in which Bering sea-ice typically retreats up to the Chukchi Sea, so in 2018 the anomalies are no longer found in Bering Sea, but there is still a significantly low sea-ice state in the Chukchi Sea over the Bering straight.

The climatological sea-ice in the Bering Sea reaches its maximum between March and April, with a southernmost bound around 57°N (the southern line of the purple box). In 2018 the maximum sea-ice extension was reached in early February corresponding to an advance of the melting season by 2-3 months (*Perovich et al.* 2018).

According to *Stabeno and Bell* (2019), Bering sea-ice is favoured by the cold northerly winds that dominate between November to March. These conditions were not dominant during most of the winter 2017/18. In November 2017 southerly warm wind delayed the arrival of the ice. Only during the next two months the northerly winds prevailed, but were warmer than usual. February and March were dominated by southerlies, pushing the sea-ice edge north and warming the surface air masses. Finally, between late March and May wind direction were relatively normal, but the warmer ocean and air conditions in the Pacific and the beginning of the natural melting season kept the low sea-ice conditions.

The southerly winds during March were driven by a sea level pressure dipole in both sides of the Bering straight, with higher pressures on the east of the straight and

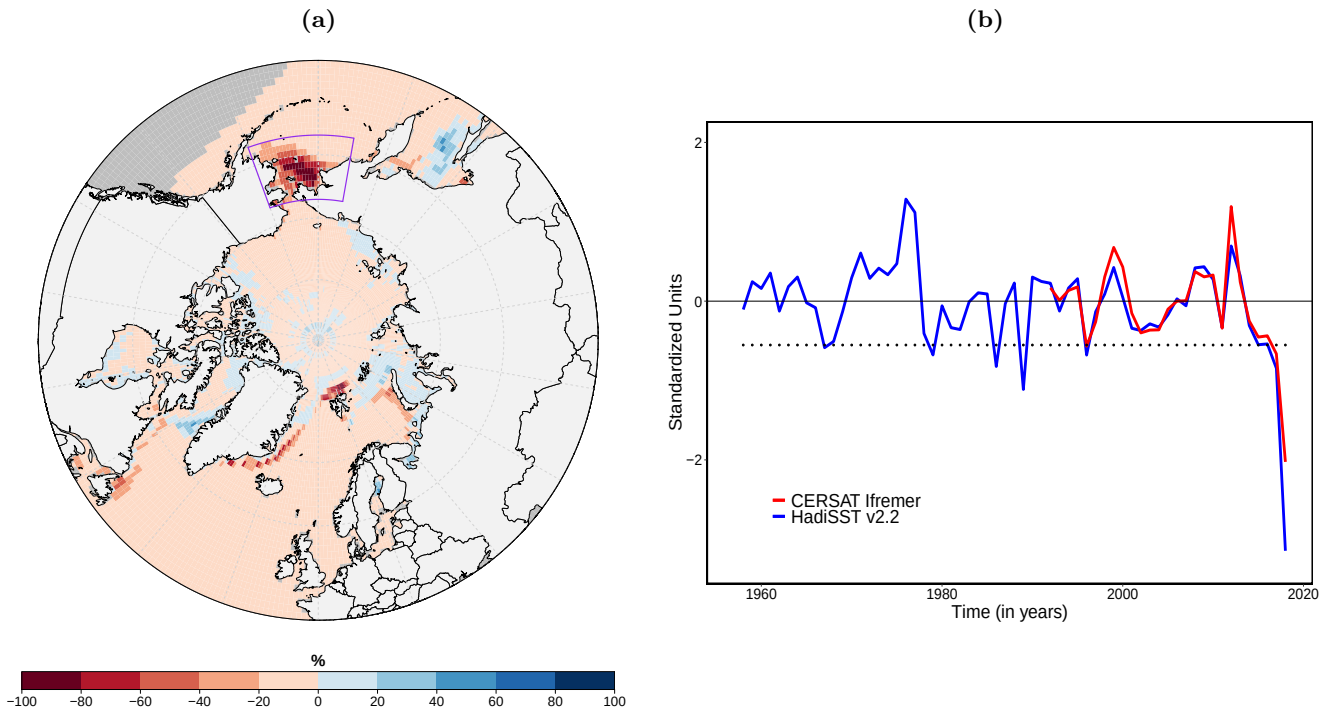

Figure 1. (a) Spatial pattern of the mean sea-ice concentration anomaly in March and April of 2018, calculated with respect to the climatology of 1992-2017 in the SSM/I CERSAT dataset. Dashed lines indicate the longitudes and latitudes grid at 20° and 10° separation respectively. (b) Time series of the standardized sea-ice concentration mean anomaly in March-April in the Bering sea (purple box on the panel on the left) for HadISST and SSM/I CERSAT. The reference period is 1958-2017 and 1992-2017, respectively. The horizontal dashed line sets the 10^{th} percentile of the HadISST timeseries, the threshold for identifying low sea-ice events in the composite analysis.

lower on the west. This pattern can also be seen in the mid-troposphere in Figure 2a, during the months of March and April. The geopotential height at 500 hPa (z500) shows the same dipole but less intense than the sea level pressure field. The effect of the warmer ocean and air temperatures with positive z500 anomalies over the northern Pacific can also be seen in the same figure.

2. Evolution of atmospheric conditions

The analyzed event (described in detail in section 1), was a large-scale drought and heatwave associated with a persistent blocking pattern in Scandinavia that lasted from April to August. It affected principally northern and central Europe, depending on the position of the blocking. We now describe the evolution of the atmosphere, and the associated regional climate signals that occurred during the following months.

Figure 2 shows the evolution of the z500 anomaly in bimonthly periods from March-April to June-July, which corresponds to 0 to 3 months after the occurrence of the sea ice anomaly in figure 1. For lags 1 to 3 a positive z500 anomaly established over Scandinavia. During April-May the blocking was more extended, covering also eastern Europe and reaching the southern and central part of the continent. One month later, the high pressure cell shifted west, covering southern Scandinavia, the UK, and northern Central Europe. Finally, in June and July, the blocking was more localised in an area around the North Sea. During all this period the anomaly reached values of 100 gpm above the climatological mean, making it a very persistent and intense blocking.

The blocking pattern was also observed in sea-level pressures (not shown), but the signal is noisier than in the mid-troposphere. We chose to show z500 precisely to minimise the noise from surface interactions, and focus on the signal that relates to the large-scale atmospheric circulation itself.

It is important to remark that during the particular month of March, the atmospheric circulation was radically different; an extremely negative NAO event prevailed during almost all the month. Figure 2a shows some clear features of this distinctive pattern, with a large negative z500 anomaly in the west coast of the European continent reaching the Iberian peninsula and high pressures North of Iceland. According to *Ayarzagüena et al.* (2018), this persistent situation was induced by a sudden stratospheric warming that happened in mid-February; it induced extremely wet conditions over southern Europe and brought to an end the 2016/2017 drought in the Iberian peninsula. Due to these strong signals, unre-

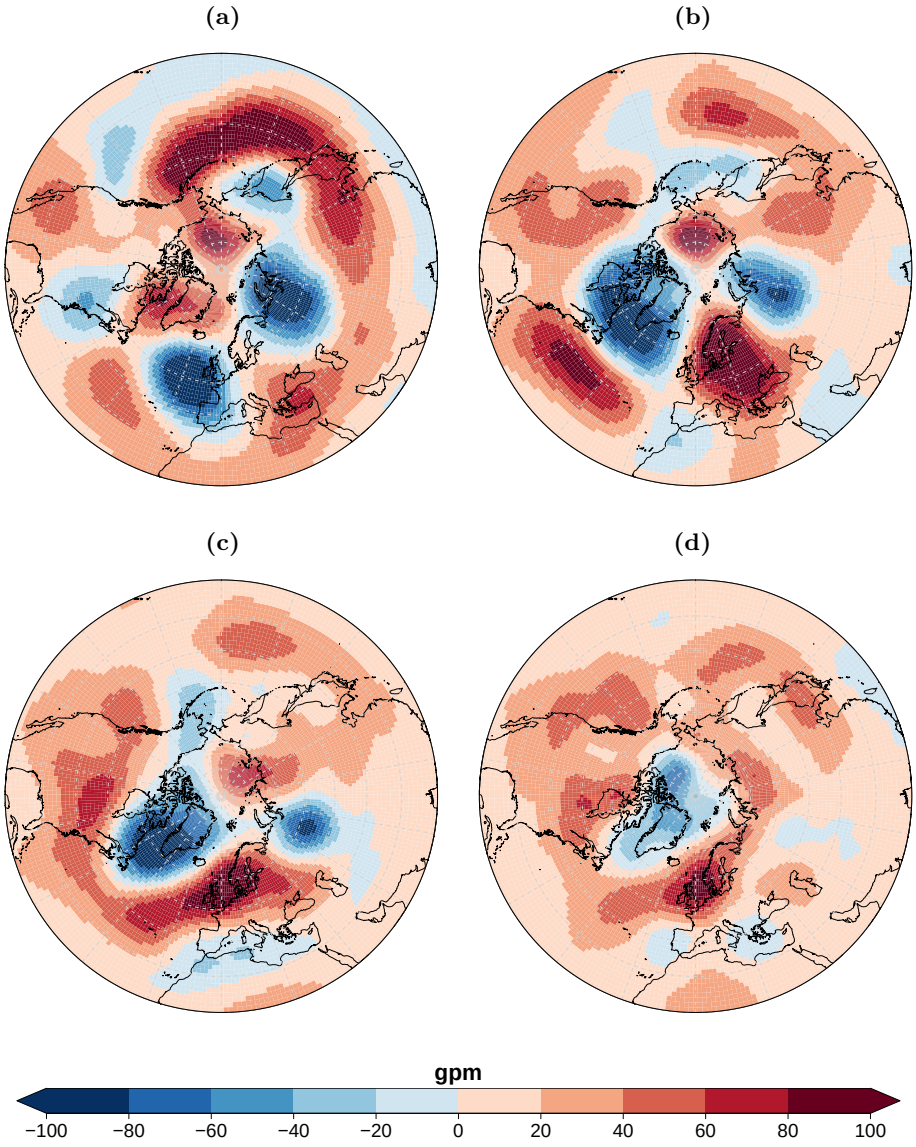

Figure 2. Spatial pattern of the mean geopotential height anomaly at 500 hPa (z500, in gpm) with respect to the climatology of 1958-2017 in the JRA-55 dataset, for: (a) March-April of 2018 (lag 0 with respect to sea ice conditions in Figure 1a); (b) April-May of 2018 (lag 1); (c) May-June of 2018 (lag 2); (d) June-July of 2018 (lag 3). Dashed gray lines indicate the longitudinal and latitudinal grid in regular intervals of 20^{o} and 10^{o}, respectively.

lated to the Scandinavian blocking, March has been deliberately left aside in the analysis of the sea-ice driven climate impacts. This is the main reason to base the plots on lagged bi-monthly averages.

The climate signals accompanying the persistent blocking are illustrated in figure 3a-c for May-June. Areas affected by the associated high pressures, where clear skies and stable conditions are predominant allowing for higher solar radiation at the surface, exhibit below-average precipitation and above-average surface temperature. This can be clearly seen in figure 3a-c, in which the area with the lowest precipitation anomalies and warmest temperatures was co-located almost perfectly with the high pressure system. The precipitation for that period (May-June) in Northern and Central Europe dropped under 50% of the climatological levels, whereas in the Mediterranean rainfall was almost two times stronger than usual. The northern region was also affected by extreme temperatures exceeding between 2 and even 3 standard deviations above the mean for May-June. These exceptionally high surface temperatures in Northern Europe, the hottest on record for the months of April-May, May-June and June-July, were likely enhanced by the dry conditions and the associated soil-moisture feedbacks.

These warm and dry conditions persisted between April and July, leaving a clear drought signal over the region. In the southern part of Europe, precipitation was much more variable, but remained above average values.

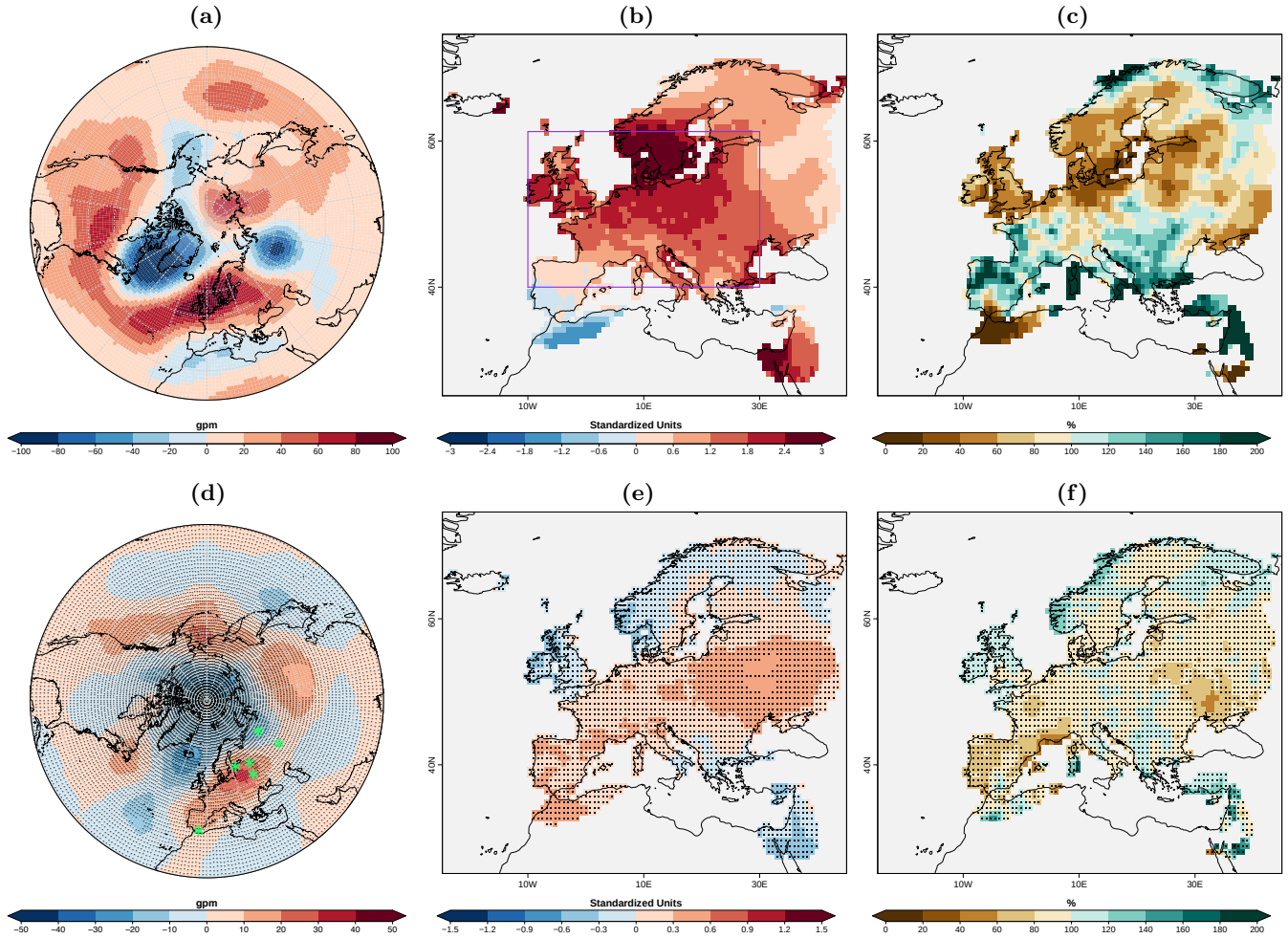

Figure 3. (a) Spatial pattern of the mean geopotential height anomaly at 500 hPa (z500; in gpm) in May-June of 2018 (lag 2 with respect to sea ice conditions in Figure 1a), calculated with respect to the climatology of 1958-2017 in the JRA-55 dataset. Dashed gray lines indicate the longitudinal and latitudinal grid in regular intervals of 20° and 10°, respectively. (b) The same as in *a* but for the standardized surface temperatures in May-June of 2018 (lag 2), calculated with respect to the climatology of 1958-2017 in the E-OBS version 19.0e dataset. The purple box is the area averaged in Figure 4 and 5. (c) The same as in *a* but for the mean precipitation anomaly for May-June of 2018, expressed as a percentage with respect to the climatology of 1958-2017 in the E-OBS version 19.0e dataset. (d) Spatial pattern of the composite mean z500 in May-June (lag 2) during the low-sea ice events, calculated with respect to the climatology for 1958-2017 in the JRA-55 data set. Black dots indicate values that are not statistically significant at the confidence level of α=0.05. The green stars mark the location of the maximum z500 value reached across Europe (15W-60E; 30N-70N) for each of the years contributing to the composite. (e-f) The same as in *d* but for the composite of the standardised surface temperatures and the mean precipitation anomaly in May-June, respectively. They are based on the same datasets as in *b,c.*

In the next section we will investigate if the exceptional anomalies in Bering sea ice and European climate here described are connected, by identifying and analysing similar SIC events and the subsequent atmospheric signals.

B. Climate signals during similar low Bering sea ice events

To explore the links between the sea-ice and the weather in Europe, we perform composite analyses around the six years with the lowest SIC values in March-April in the Bering Sea (the six for which the blue line in Figure 1b is below the dashed horizontal line). We first analyze the z500 composite anomaly, which describes the typical atmospheric circulation pattern following the six selected events. For simplicity, only the composites for May-June are included in figure 3, when the signals are found to be stronger.

The 0-month delay composite for z500 (not shown), which corresponds to the same period as the low SIC anomalies, has a significant positive anomaly above the Bering sea area. This is the expected atmospheric re-

sponse that results from an extensive sea-ice reduction, that enables larger fluxes of heat and moisture into the atmosphere, thus affecting the mid-troposphere thickness. In the 1,2 and 3-month delayed composites there is a significant blocking pattern over Europe, with anomalies that are consistently significant above the confidence level α=0.05; for the 1-month delayed (not shown) its composited center of action is located over eastern Europe, above the Black Sea, for the 2-month one a little bit further north, around the Baltic countries (Figure 3d), and for the 3-month (not shown) over the Celtic Sea. The location of the blocking in the composites is close but not exactly the same as in 2018 (Figure 3a,d), which might reflect that the exact position is sensitive to other influences and/or weather noise. Indeed, the maximum in z500 over Europe (15W-60E; 30N-70N) is in a different place for each of the six selected years, although it tends to happen in northeastern Europe (green stars in Figure 3d), where the blocking signal in 2018 occurred. Note also that positive anomalies of the composites are not as intense as in 2018, as they result from the averaging of six different years, which leads to smoothed values as the z500 maxima are not located in the same area.

In the temperature composites, significant warm anomalies are found in the areas where the blocking pattern is established. For example, in the 2-month delayed composite (Figure 3e) these are observed in a small area in eastern Europe. This is displaced with respect to the region with the warmest temperatures in May-June 2018, but is consistent with the displacement in the composited blocking cell with respect to the 2018 one. It has already been pointed out that not all the years selected to build the composites represent the blocking in the same place, which might explain the relatively low composite anomalies at the local scale. To assess the extremeness of the temperature signals, this problem can be partly circumvented by considering temperature averages at the European scale (i.e. 40-61.3N; 10W-30E, purple box in Figure 3b). In Figure 4 we show these averages for the individual years conforming the composite (blue dots), for the composite itself (blue star) and for 2018 (grey star), and compare them with the complete distribution of values for all the years between 1958 to 2017 (green box and whisker plot).

In April-May, May-June and June-July the 2018 anomaly stands out, showing larger values than for any other year in the observations. This is not the case for the low sea ice composites, for which the mean value remains positive for all lags, but also rather small. Yet, we can still highlight that for May-June and June-July, two of the individual composited years had extremely warm values close to the 2018 state. For the first, the two hottest years on record after 2018, and for the second, the hottest year and the fifth hottest after 2018.

The spatial patterns of precipitation following the low sea ice events show some important discrepancies with respect to the corresponding pattern of 2018 (Figure 3c,f). Only the 2 and 3-month delayed composites show small

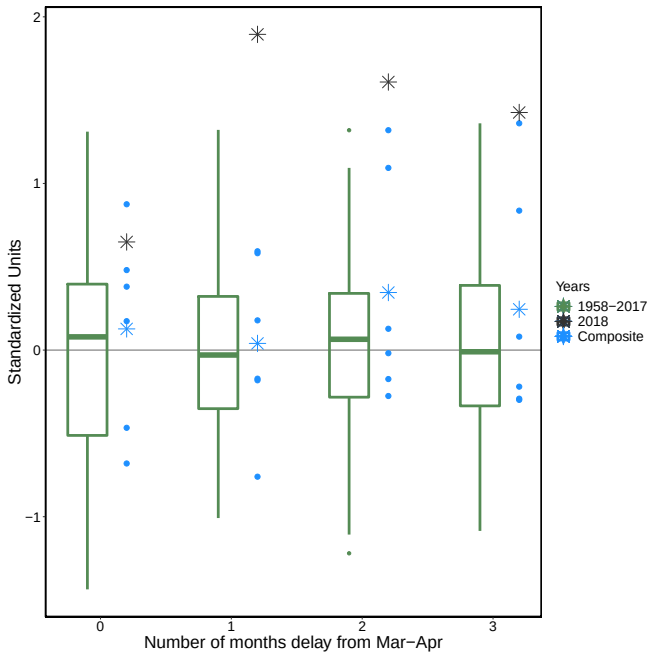

Figure 4. Box and whisker plot of the standardized surface temperature anomaly averaged over Europe (40-61.3N; 10W-30E, purple box in Figure 3b) for every March-April (lag 0), April-May (lag 1), May-June (lag 2) and June-July (lag 3) from 1958 to 2017. Anomalies are computed with respect to the climatology of the whole period, and based on the E-OBS dataset v19.0e. The blue stars correspond to the corresponding value for the low Bering sea ice composite, the blue dots to those of the composited individual years, and the black star to the one for 2018. In the box whisker plot, the box stretches between the percentile 25 and the percentile 75, and the whiskers extend from the box to the largest/smallest value, without exceeding 1.5 times the inter-quartile range. Outliers are plotted as green dots.

regions with significantly reduced precipitation (as compared to climatology) in Eastern Europe, also present in 2018. However, significant values are also observed in other regions, like the Gulf of Lion that shows dry conditions in stark contrast to the increased precipitation that occurred in 2018. These differences reflect that precipitation follows a more irregular distribution than temperature, which may be due to the fact that it is more sensitive to internal variability. To reduce this effect, we averaged precipitation anomalies at the European-scale, in the same way that it has been done by the temperature anomalies.

In figure 5, for the 0-month delay, in which no influence over Europe is expected, the individual composite years are distributed almost evenly between high and low precipitation values. One month later, four out of the six selected years show precipitation conditions near average and only one shows comparable dry conditions to 2018. It is important to remark that 2018 shows consistent dry conditions for all months, but with values that are not particularly extreme. For the composites, May-June and

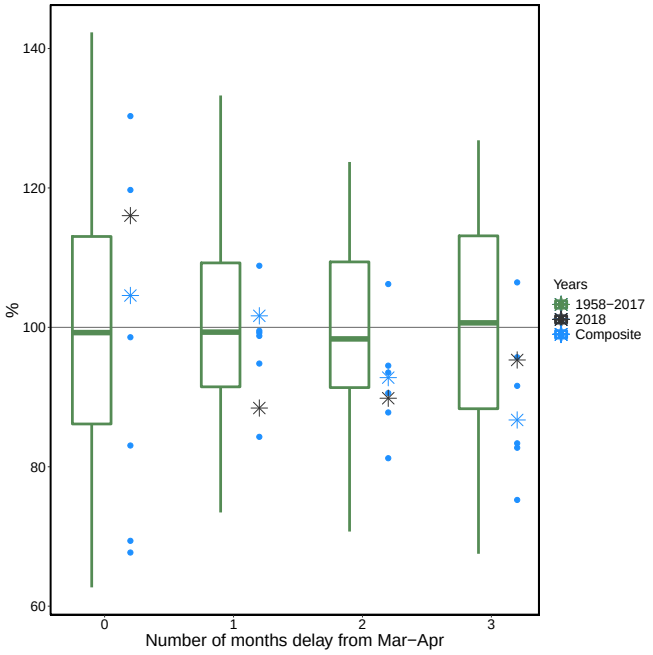

Figure 5. The same as in (Figure 4) but for the precipitation anomaly (expressed as percentage with respect to the climatology for 1958-2017) averaged over Europe (40-61.3N; 10W-30E, purple box in Figure 3b). It is based in the E-OBS dataset v19.0e.

June-July show predominantly dry conditions, with three of the selected years showing values below the percentile 25, and only one experiencing above average precipitation. This result, together with the analysis from figure 4 suggests that low sea ice conditions in the Bering Sea in March-April can lead to reduced precipitation and warmer conditions at the European scale 2 to 3 months later.

IV. CONCLUSIONS

In this study, we have been able to analyze and contextualize the extreme events in the Bering Sea and Central and Northern Europe during the first half of 2018. In order to investigate potential linkages between these two regions, we have identified analogue events of low sea-ice in the Bering Sea and analyzed the common subsequent signals over Europe. Based on the results derived from the analysis presented in this work, we can conclude that:

- Two observational records support that the anomalous sea-ice reduction in the Bering Sea between January and April of 2018 was record-breaking.

- A persistent blocking pattern over Scandinavia was identified between April and July of the same year, and found to be consistent with the widespread drought and heatwave in Europe, which were unprecedented both in terms of extremeness and persistence.

- A composite built for the six lowest sea-ice years in Bering Sea after 2018 shows a similar blocking pattern over Europe starting one month after the sea-ice anomalies are established and persisting during the next three months. However, the position of the centers of action of the blocking of the individual years vary and not all the years the blocking is located in the same position.

- The composite analysis also exhibits significant hot and dry conditions over Eastern Europe co-located with the blocking pattern, thus supporting the the same relation observed between them in 2018. Some spatial differences are seen with respect to 2018, which could be accounted by internal variability and its interactions with the location of the blocking.

Given that the strongest sea-ice signal was in 2018, it was not possible to identify completely analogous events in the observational record, and therefore assess if the magnitude of the event played a key role in the remarkable climate signals over Europe.

As future work, complementary analyses could be done using model simulations tailored to inference causality, e.g. by prescribing specific sea ice conditions and contrasting the atmospheric response to that of a climatology, as well as to investigate the teleconnection mechanisms. These simulations can be idealised to circumvent the typical problems of observations, such as the shortness of the study period, or inconsistencies between the datasets employed for each variable (e.g. satellite products vs reanalyses). It is important, however, to keep in mind that models can be biased, and fail to represent key aspects of the real world.

Finally, to summarise our findings, we note that this study has found a statistically significant link between the circulation over Europe and the preceding Bering sea-ice state in early spring. Further work with models will try to shed light on the causality in this relationship, and the mechanism connecting these events. Nevertheless, we can state, disregarding the causality, the existence of such a relationship implies that Bering sea-ice could be used as a predictor of the weather in Europe.

ACKNOWLEDGMENTS

I would like to thank Dr. Pablo Ortega, Dr. Juan C. Acosta, Dr. Markus G. Donat and Dr. Simon Wild for introducing me to the world of the climate research, and for their patience and guidance in developing this project. It has been a pleasure to work with them and to be part during this time of the Earth Sciences department at the BSC. I also want to thank Dr. Raül Marcos from the University of Barcelona for his comments.

Finally, none of this could have happened without the help from my family, friends, and particularly Alba; not only from those who shared the technical and practical knowledge and helped me with the difficulties I faced but to those who helped in the best way they could despite having no experience in the subject.

REFERENCES

Acosta Navarro, J. C., P. Ortega, J. García-Serrano, V. Guemas, E. Tourigny, R. Cruz-García, F. Massonnet, and F. J. Doblas-Reyes, December 2016: Linking the lowest arctic sea-ice extent on record with the lowest european precipitation event on record, *Bulletin of the American Meteorological Society*, *100*(1), S43–S48, 2019.

Agora Energiewende and Sandbag, The european power sector in 2018. Up-to-date analysis on the electricity transition., 2019.

Ayarzagüena, B., D. Barriopedro, J. M. Garrido-Perez, M. Abalos, A. de la Cámara, R. García-Herrera, N. Calvo, and C. Ordóñez, Stratospheric connection to the abrupt end of the 2016/2017 iberian drought, *Geophysical Research Letters*, *45*(22), 12,639–12,646, doi: 10.1029/2018GL079802, 2018.

Barnes, E. A., Revisiting the evidence linking arctic amplification to extreme weather in midlatitudes, *Geophysical Research Letters*, *40*(17), 4734–4739, doi:10.1002/grl.50880, 2013.

Budikova, D., Role of arctic sea ice in global atmospheric circulation: A review, *Global and Planetary Change*, *68*(3), 149–163, 2009.

Burger, B., High solar power production ensures stable electricity supply, Fraunhofer Institute for Solar Energy Systems ISE. https://www.ise.fraunhofer.de/en/press-media/news/2018/high-solar-power-production-ensures-stable-electricity-supply.html, Accessed: 2020-01-06, 2018.

Copernicus, European state of the climate 2018., https://climate.copernicus.eu/ESOTC, 2019.

Efron, B., and R. Tibshirani, Bootstrap methods for standard errors, confidence intervals, and other measures of statistical accuracy, *Statistical science*, pp. 54–75, 1986.

Francis, J. A., and S. J. Vavrus, Evidence linking arctic amplification to extreme weather in mid-latitudes, *Geophysical Research Letters*, *39*(6), doi:10.1029/2012GL051000, 2012.

Haylock, M. R., N. Hofstra, A. M. G. Klein Tank, E. J. Klok, P. D. Jones, and M. New, A european daily high-resolution gridded data set of surface temperature and precipitation for 1950–2006, *Journal of Geophysical Research: Atmospheres*, *113*(D20), doi:10.1029/2008JD010201, 2008.

Kobayashi, S., et al., The jra-55 reanalysis: General specifications and basic characteristics, *Journal of the Meteorological Society of Japan. Ser. II*, *93*(1), 5–48, doi: 10.2151/jmsj.2015-001, 2015.

Kornhuber, K., S. Osprey, D. Coumou, S. Petri, V. Petoukhov, S. Rahmstorf, and L. Gray, Extreme weather events in early summer 2018 connected by a recurrent hemispheric wave-7 pattern, *Environmental Research Letters*, *14*(5), 054,002, 2019.

Manubens, N., et al., An r package for climate forecast verification, *Environ. Model. Softw.*, *103*(C), 29–42, doi: 10.1016/j.envsoft.2018.01.018, 2018.

NASA Earth Observatory, Scarcely Seen Scandinavian Fires, https://earthobservatory.nasa.gov/images/92454/scarcely-seen-scandinavian-fires., Accessed: 2020-01-06, 2018.

Note1, Data made available by CERSAT/IFREMER (Institut français de recherche pour l'exploitation de la mer) at: ftp://ftp.ifremer.fr/ifremer/cersat/products/gridded/psi-concentration/, Accessed: 2019-09-14.

Overland, J. E., and M. Wang, Large-scale atmospheric circulation changes are associated with the recent loss of arctic sea ice, *Tellus A*, *62*(1), 1–9, doi:10.1111/j.1600-0870.2009.00421.x, 2010.

Perovich, D., et al., Sea ice [in arctic report card 2018], https://arctic.noaa.gov/Report-Card/Report-Card-2018/ArtMID/7878/ArticleID/780/SeanbspIce, 2018.

R Core Team, R: A language and environment for statistical computing, https://www.R-project.org/, 2019.

Screen, J. A., and I. Simmonds, Caution needed when linking weather extremes to amplified planetary waves, *Proceedings of the National Academy of Sciences*, *110*(26), E2327–E2327, 2013a.

Screen, J. A., and I. Simmonds, Exploring links between Arctic amplification and mid-latitude weather, *Geophysical Research Letters*, *40*(5), 959–964, doi:10.1002/grl.50174, 2013b.

Screen, J. A., and I. Simmonds, Amplified mid-latitude planetary waves favour particular regional weather extremes, *Nature Climate Change*, *4*(8), 704, 2014.

Stabeno, P. J., and S. W. Bell, Extreme conditions in the bering sea (2017–2018): Record-breaking low sea-ice extent, *Geophysical Research Letters*, *46*(15), 8952–8959, doi: 10.1029/2019GL083816, 2019.

Thoman JR, R. L., et al., The record low bering sea ice extent in 2018: Context, impacts, and an assessment of the role of anthropogenic climate change, *Bulletin American Meteorological Society: Explaining Extreme Events of 2018 from a Climate Perspective*, pp. S15–S19, 2019.

Toreti, A., et al., The exceptional 2018 european water seesaw calls for action on adaptation, *Earth's Future*, *7*(6), 652–663, doi:10.1029/2019EF001170, 2019.

Yiou, P., J. Cattiaux, D. Faranda, N. Kadygrov, A. Jézéquel, et al., Analyses of the northern european summer heatwave of 2018, *Bulletin American Meteorological Society: Explaining Extreme Events of 2018 from a Climate Perspective*, 2019.